Journal of Neuroradiology 46 (2019) 44–51

Available online at ScienceDirect www.sciencedirect.com

Elsevier Masson France EM|consulte www.em-consulte.com

Original Article

Consistency of normalized cerebral blood volume values in glioblastoma using different leakage correction algorithms on dynamic susceptibility contrast magnetic resonance imaging data without and with preload

Dennis Hedderich[a,1], Anne Kluge[a,1,2], Thomas Pyka[b], Claus Zimmer[a], Jan S. Kirschke[a], Benedikt Wiestler[a], Christine Preibisch[a,c,*]

[a] Department of Diagnostic and Interventional Neuroradiology, Technische Universität München, Ismaningerst. 22, 81675 Munich, Germany
[b] Clinic for Nuclear Medicine, Technische Universität München, Ismaningerst. 22, 81675 Munich, Germany
[c] Clinic for Neurology, Technische Universität München, Ismaningerst. 22, 81675 Munich, Germany

ARTICLE INFO

Article history:
Available online 21 May 2018

Keywords:
DSC-MRI
Normalized CBV
Leakage correction
Human glioma

ABSTRACT

Background and purpose. – Several leakage correction algorithms for dynamic susceptibility contrast (DSC) magnetic resonance imaging (MRI)-based cerebral blood volume (CBV) measurement have been proposed, and combination with a preload of contrast agent is generally recommended. A single bolus application scheme would largely simplify and facilitate standardized clinical applications, while reducing contrast agent (CA) dose. The aim of this study was, therefore, to investigate whether appropriate leakage correction redundantizes prebolus application by comparing normalized DSC-based CBV (nCBV) measures of two consecutive CA boli.

Materials and methods. – Twenty-seven patients with suspected glioblastoma (WHO-grade-IV) underwent DSC-MRI during two consecutive boli of Gd-based CA. Four variants of two post-processing leakage correction techniques were compared with respect to nCBV in contrast enhancing tumor tissue. First, a reference curve approach with first pass and full integration of corrected $\Delta R2^*(t)$, and second, a deconvolution-based approach using singular value decomposition (SVD) with a standard noise-dependent cutoff or Tikhonov regularization.

Results. – Compared to respective uncorrected values, all leakage correction techniques increased nCBV for data acquired without prebolus, while there was no consistent trend for data acquired with prebolus. The best agreement between corrected nCBV values in contrast enhancing tumor, obtained in the same patients without and with prebolus, respectively, was obtained for the reference curve-based correction approach with either first pass or full integration.

Conclusion. – The reference curve-based leakage correction approach with integration-based nCBV calculation yielded a high accordance between nCBV values without and with prebolus, respectively. Thus, it appears possible to obtain valid nCBV in glioblastoma with a single CA injection.

Abbreviations: AIF, arterial input function; AUC, area under the curve; CA, contrast agent; (n)CBV, (normalized) cerebral blood volume; CET, contrast enhancing tumor; corr, corrected; DSC, dynamic susceptibility contrast; DTPA, diethylenetriaminepentacetate; EES, extravascular extracellular space; EPI, echo planar imaging; FLAIR, fluid attenuated inversion recovery; Gd, gadolinium; GE, gradient echo; GM, grey matter; MB, main bolus; MPRAGE, magnetization prepared rapid acquisition gradient echo; MRI, magnetic resonance imaging; PB, prebolus; SVD, singular value decomposition; TE, echo time; TFE, turbo field echo; TI, inversion time; TR, repetition time; unc, uncorrected; VOI, volume of interest; WM, white matter.

* Corresponding author at: Klinikum rechts der Isar der TU München, Department of Diagnostic and Interventional Neuroradiology, Ismaninger Straße 22, 81675 München, Germany.
E-mail address: preibisch@tum.de (C. Preibisch).
[1] These authors contributed equally.
[2] Present address: Charité CyberKnife Center, Campus Virchow-Klinikum, Augustenburger Platz 1, 13353 Berlin, Germany.

https://doi.org/10.1016/j.neurad.2018.04.006
0150-9861/

Introduction

Dynamic susceptibility contrast (DSC) magnetic resonance imaging (MRI) is an integral part of recent multi-parametric MRI protocols and derived cerebral blood volume (CBV) is increasingly used in diagnostic imaging, especially for characterizing brain tumors [1]. In general, the technique is expected to be able to delineate metabolically active tumor tissue via elevated CBV values. Recently, the American Society of Functional Neuroradiology (ASFNR) put forth recommendations for DSC-based CBV measurement, which is used clinically to establish the diagnosis of intracranial neoplasm and to further characterize its etiology (e.g. ganglioma, medulloblastoma, metastasis, glioma) [2,3] as well as to predict WHO grade in gliomas [4]. Using multi-parametric MRI and a machine learning approach, a recent study showed that the standard deviation of CBV is one of the most important features in predicting tumor grade [5]. Additionally, CBV maps acquired from DSC-MRI can be helpful for evaluating therapy response in glioma and to distinguish tumor progression from pseudo-progression or radiation necrosis [4,6,7].

At the current state, DSC-based perfusion imaging is hampered by the fact that standards, as proposed by the ASFNR [4], are not yet commonly used, which certainly accounts for the variable outcomes of clinical studies [8]. This problem is exacerbated by the fact that in regions with disrupted blood brain barrier, resulting CBV values are severely confounded by contrast agent leakage into the extravascular extracellular space (EES). Depending on whether T1- or T2*-related leakage effects dominate, CBV can be either under- or overestimated [9–14]. To alleviate that problem, application of a prebolus has been proposed to reduce T1-related leakage effects [15]. Currently, application of a contrast agent preload prior to DSC-MRI, together with appropriate processing for leakage correction [9,11], is quite accepted to improve accuracy in DSC-based CBV mapping [4,10,16–18]. Nevertheless, a recent study demonstrated that even after prebolus application CBV results of three different leakage correction techniques differed, depending on whether T1- or T2*-related relaxation effects dominated in the EES [13]. Considering aspects of time efficiency and ease of application, accurate CBV mapping using a single dose of contrast agent received renewed attention also with respect to minimizing the dose of applied contrast agent.

In order to explore the reliability of single dose DSC-based CBV mapping, we performed a prospective study, where DSC-MRI data were acquired in 27 patients with suspected glioblastoma during the injection of two consecutive boli of contrast agent (prebolus, main bolus). To investigate the influence of postprocessing on normalized CBV (nCBV) values, four optimized variants of two different leakage correction approaches, based on reference curves and relaxation curve integration (area under the relaxation curve, AUC) and singular value decomposition (SVD) have been applied and compared with respect to consistency.

Material and methods

Patients and instrumentation

The study was approved by the local ethics committee and conducted in accordance with approved guidelines. Twenty-seven patients with suspected high-grade glioma were recruited for this study and provided written informed consent. Data of 20 patients (58.4 ± 16.9 years, 13 males) could be evaluated for the presented study; seven patients had to be excluded because of other diagnoses ($n = 4$), technical problems ($n = 1$) or motion ($n = 2$) in the DSC-based CBV measurement.

Patients were examined at 3 T, either on a Biograph mMR scanner (Siemens Medical Solutions, Germany) or on an Achieva System (Philips Healthcare, Best, The Netherlands).

DSC MRI

Two sets of DSC-MRI data were obtained from each patient: (1) during injection of a standardized prebolus (PB) dose of 7.5 ml (≈ 0.05 mmol/kg) and (2) during injection of a main bolus (MB) of 15 ml (≈ 0.1 mmol/kg) of Gd-containing contrast agent (Gd-diethylene-triamine-pentacetate (DTPA) or Dotarem). In each case the bolus was injected by means of a power injector (Medrad Spectris Solaris EP, Bayer Medical Care, Whippany, NJ) at a rate of 4 ml/s followed by 20 ml of saline solution (at 4 ml/s), with a minimum delay of 3 min between injections. MRI acquisition employed single-shot gradient-echo (GE) echo planar images (EPI) (TE/TR/α = 30 ms/1500 ms/90°, 20/25 slices, voxel sizes $1.8 \times 1.8 \times 4\,mm^3$/$1.75 \times 1.75 \times 4\,mm^3$, gap 1 mm/0 mm). Eighty dynamic images were acquired for each time series to ensure sufficient coverage for application of leakage correction techniques [13]. For each patient 3D fluid attenuated inversion recovery (FLAIR; TE/TR/TI = 301 ms/4800 ms/1650 ms, voxel size $1.12 \times 1.12 \times 1.12\,mm^3$) and post-contrast 3D T1-weighted magnetization prepared rapid acquisition gradient echo (MPRAGE; TE/TR/α = 4 ms/9 ms/8°, TI/TFE shot interval = 900 ms/1745 ms, voxel size $1 \times 1 \times 1\,mm^3$) data were acquired within an advanced diagnostic tumor imaging protocol.

CBV evaluation

Two types of leakage correction techniques were investigated: One approach estimates leakage contributions from linear combinations of healthy tissue reference curves [11] and calculates CBV via integration of the transverse relaxation rate changes $\Delta R2^*(t)$ (AUC, area under the curve). The other approach derives a flow and extravasation-weighted residue function $R(t)$ using a matrix formulation of the deconvolution theorem, which is solved by singular value decomposition (SVD) and determines leakage information from the tail of $R(t)$ [9]. For the current study, we implemented two variants of each technique using modifications as described by [13], resulting in uncorrected (unc) and corrected (corr) CBV parameter maps for a total of four method variants. Specifically, to investigate the influence of integration range on AUC-based CBV measures, first pass AUC and full AUC CBV values were obtained by integrating only the first pass or the full range (full) of the relaxation time curve, $\Delta R2^*(t)$, respectively. Since the known noise sensitivity of the SVD algorithm [19] can be mitigated by different approaches, we implemented two different regularization techniques to compare their performance. First, for standard regularization (standard SVD) a global SNR dependent cut-off was used as implemented before [13] and recommended by Knutsson et al. [14]. Second, Tikhonov regularization (Tikhonov SVD) [12] was implemented combining the L-curve criterion [20] with a small SNR-dependent cut-off [21].

Prior to any processing, DSC data were checked for image quality and motion. According to that, three patients needed to be excluded because of severe motion ($n = 2$) and missing contrast agent ($n = 1$). From the remaining 20 data sets, data quality was rated as high ($n = 7$), good ($n = 6$), acceptable ($n = 4$) or low ($n = 5$) according to overall appearance (patient motion, intensity fluctuations, signal drop). CBV evaluation was then performed using custom programs implemented in Matlab R2016b (MathWorks, Natick, US), employing standard SPM12 (http://www.fil.ion.ucl.ac.uk/spm) routines with default settings for data coregistration and segmentation. First, DSC time courses were converted to $\Delta R2^*(t)$ and smoothed with a Gaussian convolution kernel ($3 \times 3 \times 3$ voxel) with the 3rd dimension in time. Anatomical FLAIR and MPRAGE data were

segmented for white matter (WM), grey matter (GM) and cerebrospinal fluid (CSF) and registered to the first image of the DSC time course.

For the AUC method, the healthy tissue reference curve $\left(\overline{\Delta R2^*(t)}\right)$ was determined by averaging $\Delta R2^*(t)$ within tissue segments of healthy GM and WM (both probability > 0.75) after tumor affected tissue areas have been subtracted. To this end, leakage and edematous areas have been determined using an automated histogram-based approach (see [13] for details). $\left(\overline{\Delta R2^*(t)}\right)$ was then used to obtain the leakage related permeability parameter K_2 by voxel wise fitting of $\Delta R2^*(t)$ (see Eq. [1] in [13]), where positive and negative K_2 values allowed accounting for T1 ($K_2 > 0$) and T2* ($K_2 < 0$) related leakage effects. Using $\left(\overline{\Delta R2^*(t)}\right)$ and K_2, corrected relaxation curves $\Delta R2^*_{corr}(t)$ were then calculated from the original $\Delta R2^*(t)$ (see Eq. [2] in [13]). Corrected and uncorrected CBV parameter maps were then calculated by numerical trapezoidal integration of $\Delta R2^*_{corr}(t)$ and $\Delta R2^*(t)$ (see Eq. [4] in [13]). The integration intervals were automatically determined from the healthy tissue reference curve and set identical for all voxels of one patient. Integration started three time points before $\left(\overline{\Delta R2^*(t)}\right)$ increased; the upper limit was either set three time points after the numerically determined end of the first pass (first pass integration) or to the end of acquisition interval (full integration).

In order to increase reproducibility of the deconvolution-based approach, an arterial input function (AIF) was selected fully automatically using a SVD approach [21]. Voxel wise SVD-based deconvolution of the relaxation time curves $\Delta R2^*(t)$ with the arterial input function was then performed using standard as well as Tikhonov regularization. Uncorrected CBV values were obtained for both cases (standard SVD and Tikhonov SVD) via full range integration of the impulse response function $H(t) = CBF \cdot R(t)$ (see Eq. [5] in [13]). For leakage correction, the residue function was fit by a Lorentzian function [9] to obtain the capillary transit time T_c for each voxel. K_2 was then calculated by averaging the tail of the impulse response function for $t > 8 \cdot T_c$, or at least 10 time points [21]. Corrected CBV values were then obtained for both regularization approaches (standard SVD and Tikhonov SVD) by adding a K_2-dependent leakage term (see Eq. [6] in [13]).

For comparability, all CBV values of one patient were normalized to a healthy white matter segment (WM probability > 0.9, tumor affected areas subtracted) assuming $CBV_{WM} = 2.5$ % [22,23], resulting in normalized CBV (nCBV) values for all investigated processing variants.

In order to investigate the influence of data quality on the performance of leakage correction, qualitative ratings of corrected nCBV maps (rater C.P.) and standard deviations of corrected nCBV in healthy GM and WM were correlated with percent signal drop, length and SNR of pre- and post-bolus baseline, as well as maximum translation and rotation obtained from motion correction (see supplement for details).

Data analysis and statistics

For volume of interest (VOI) evaluation, healthy GM and WM masks were derived for each individual patient by thresholding ($P_{WM} > 0.75$, $P_{GM} > 0.75$) tissue segments generated by SPM12 and removing tumor areas using the same histogram based approach described above for detection of tumor affected tissue [13]. Contrast enhancing tumor tissue (CET) was semi-automatically segmented using a threshold-based approach within ITK-Snap [24]. All segmentations were visually inspected by D.H. and B.W. and manually refined where necessary. These masks were then used to extract VOI average values in GM, WM and CET from all nCBV parameter maps for all patients. Box plots with notches are used to visualize the range and relative distribution of nCBV values obtained by different processing (first pass AUC, full AUC, standard SVD, Tikhonov SVD), leakage correction (uncorrected, corrected) and acquisition scheme (data acquisition during prebolus or main bolus). Differences of VOI average nCBV values between PB and MB data were calculated for all investigated processing methods. Patient-average nCBV values (mean ± standard deviation) for MB-derived nCBV values and their differences to PB-derived nCBV are summarized in Table 1 for all investigated methods. A paired two-sided t-test was used to test for statistically significant differences.

To better visualize the performance differences between processing methods with regard to nCBV values derived from PB and MB data, we generated Bland-Altman plots [25]. For every patient, the difference between main bolus and prebolus nCBV and the mean of the two measurements were calculated. Scatter plots were generated for every post-processing algorithm (Y-axis: difference between main bolus and prebolus; X-axis: mean of main and prebolus). For better comparability, the same scaling was chosen for the uncorrected and corrected plots of each method.

To better characterize the similarity between PB- and MB-derived nCBV values in CET for the different processing techniques, the Chi-square distance was calculated in Python 3.5, with I as an iterator over the 100 bins of the nCBV histograms:

$$d(H1, \quad H2) = \frac{1}{2}\sum_I \frac{(H1(I) - H2(I))^2}{H1(I) + H2(I)}$$

Results

Sixteen nCBV parameter maps obtained from a high quality patient data set via eight different processing variants from data acquired during application of the prebolus (i.e. without contrast agent predose) and main bolus (i.e. with contrast agent predose) are shown in Fig. 1. For comparison, the same set of nCBV parameter maps for a low quality patient data set with weak signal drop is shown in supplemental Fig. S1. It can clearly be seen that

Table 1
Patient averages ($n = 20$) of normalized CBV (nCBV) values obtained during main bolus (MB) acquisitions and differences between prebolus (PB) and main bolus (PB-MB) nCBV in healthy brain (GM and WM) and contrast enhancing tumor tissue (CET). Uncorrected (unc) and corrected (corr) nCBV values were obtained by two different methods (AUC: area under time curve, SVD: singular value decomposition) and their variants (fpAUC: first pass integration, fullAUC: full range integration, sSVD: standard truncated SVD, TiSVD: SVD with Tikhonov regularization). Statistical *P*-values for differences between nCBV values obtained from PB and MB acquisitions are based on a paired two-sided *t*-test. Insignificant differences are emphasized by bold print.

nCBV [%]	WM			GM			CET		
	MB	PB-MB	*P*	MB	PB-MB	*P*	MB	PB-MB	*P*
fpAUC, unc	**2.55 ± 0.22**	**0.01 ± 0.06**	**0.4157**	**4.20 ± 0.37**	**−0.02 ± 0.29**	**0.7725**	7.53 ± 2.56	−2.32 ± 1.29	0.0000
fpAUC, corr	**2.53 ± 0.21**	**0.01 ± 0.05**	**0.3615**	**4.15 ± 0.30**	**−0.01 ± 0.18**	**0.8147**	**7.08 ± 2.28**	**−0.05 ± 0.57**	**0.6916**
fullAUC, unc	2.58 ± 0.23	0.28 ± 0.31	0.0006	4.29 ± 0.40	0.48 ± 0.81	0.0154	8.28 ± 3.09	−5.77 ± 3.08	0.0000
fullAUC, corr	**2.53 ± 0.21**	**0.01 ± 0.05**	**0.3704**	**4.15 ± 0.29**	**0.03 ± 0.15**	**0.3432**	6.64 ± 2.23	−0.30 ± 0.65	0.0490
sSVD, unc	2.68 ± 0.27	2.00 ± 3.08	0.0093	4.55 ± 0.53	3.07 ± 4.91	0.0116	**9.36 ± 3.61**	**−4.39 ± 11.77**	**0.1116**
sSVD corr	2.58 ± 0.28	0.13 ± 0.13	0.0004	**4.13 ± 0.78**	**0.03 ± 0.62**	**0.8296**	9.52 ± 3.37	−2.78 ± 3.02	0.0006
TiSVD, unc	2.63 ± 0.25	0.80 ± 0.98	0.0017	4.42 ± 0.47	1.30 ± 1.93	0.0071	8.99 ± 3.47	−6.64 ± 3.71	0.0000
TiSVD, corr	2.60 ± 0.26	0.33 ± 0.53	0.0110	**4.28 ± 0.47**	**0.34 ± 0.96**	**0.1316**	9.77 ± 3.38	−5.46 ± 3.07	0.0000

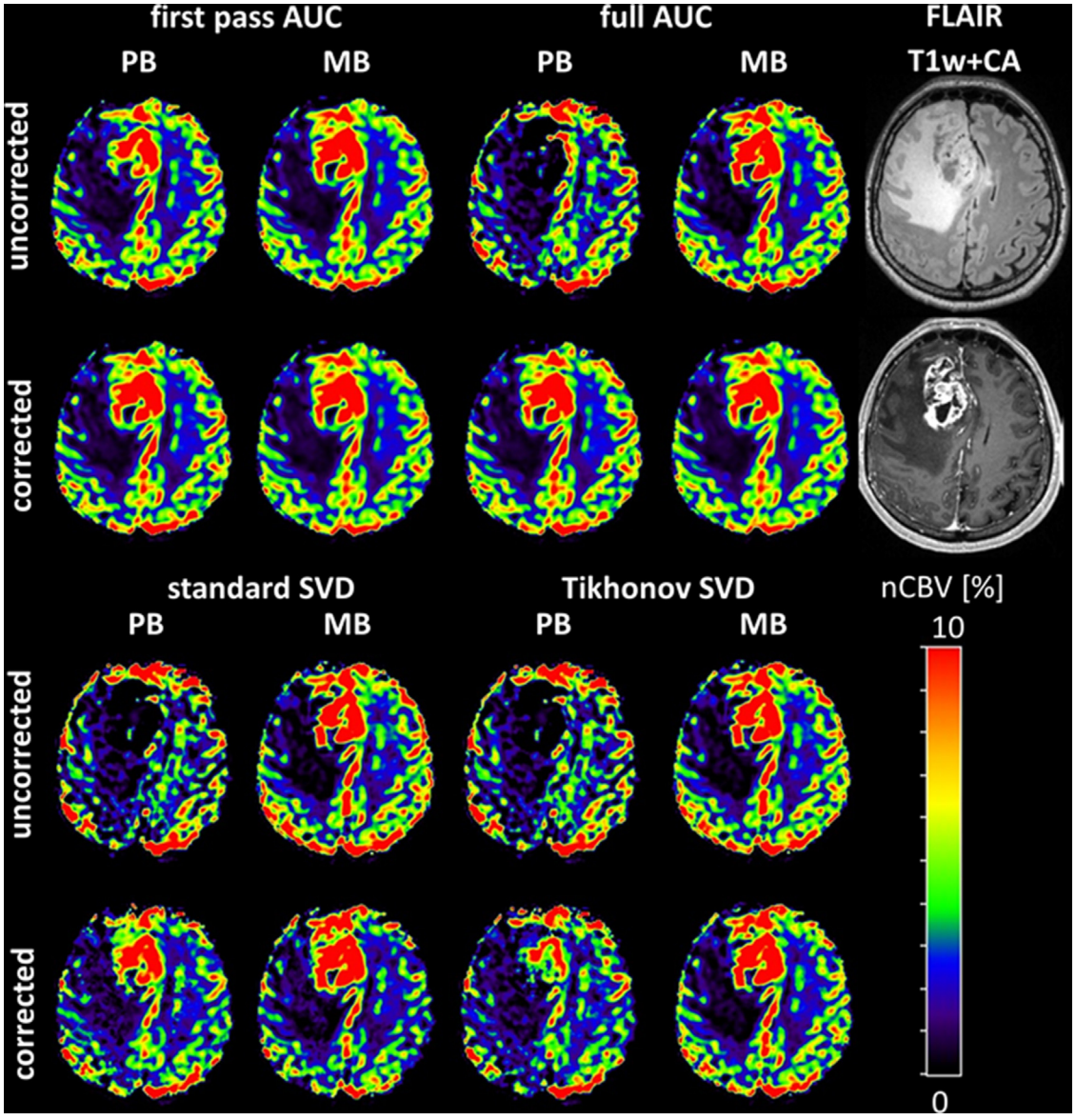

Fig. 1. Selected slice of a patient (62 years, male) with glioblastoma demonstrating nCBV maps resulting from high quality DSC data. Uncorrected and corrected normalized CBV (nCBV) parameter maps are shown for the two different methods (AUC: area under time curve, SVD: singular value decomposition) and their variants (first pass AUC: first pass integration, full AUC: full range integration, standard SVD: standard truncated SVD, Tikhonov SVD: SVD with Tikhonov regularization). In the upper right panels, T2-weigthed FLAIR and contrast enhanced T1-weighted (T1w + CA) conventional MR images of the same slice are shown for anatomical reference.

uncorrected nCBV maps acquired during PB (upper left image in each of the four panels in Figs. 1 and S1) generally show low nCBV values in contrast enhancing tumor. In all cases, at least in the high quality example, leakage correction effects a clear increase of nCBV in this area (lower left image in each of the four panels). One exception is the first pass AUC method, with minor differences between uncorrected and corrected nCBV maps (left column in left upper panel). For nCBV values obtained from MB acquisitions (right column in each of the four panels), differences between uncorrected (upper right) and corrected (lower right image in each of the four panels) nCBV parameter maps are less obvious. Overall, the spatial pattern of leakage corrected nCBV maps appears largely identical on visual inspection, where nCBV maps generated by the AUC method variants (top panels) appear less noisy than nCBV parameter maps obtained via SVD variants (bottom panels). With regard to the SVD-based nCBV, the PB-based maps clearly show inferior quality compared to MB-based maps. This effect is clearly aggravated with decreasing data quality (compare Figs. 1 and S1). From all investigated correlations between measures of data quality, the influence of signal drop on the performance of leakage correction was most significant. In our sample, patient motion and temporal SNR were not found to significantly influence quality of corrected nCBV maps. However, severely motion affected DSC data were excluded from evaluation and temporal SNR was decent in all cases (see supplement for details).

Box plots of nCBV averages in contrast enhancing tumor across all patients, demonstrate the behavior of nCBV obtained with different uncorrected (unc) and corrected (corr) processing variants (Fig. 2). It can be seen that nCBV values obtained during application of the prebolus (i.e. without predose; Fig. 2a) are indeed systematically low for uncorrected nCBV and clearly increased by all correction techniques. For nCBV values obtained during application of the main bolus (i.e. with predose; Fig. 2b), differences between uncorrected and corrected nCBV averages in CET are generally smaller and rather negligible for first pass AUC and standard SVD. Correction using the full AUC approach effects a clear decrease

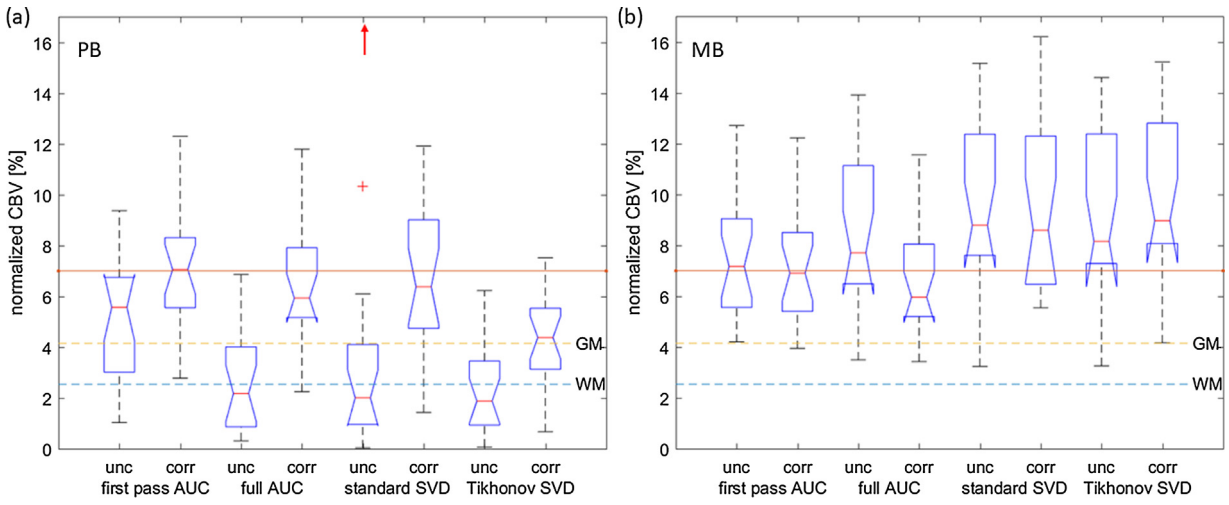

Fig. 2. Box plots of nCBV averages in contrast enhancing tumor for all patients ($n = 20$) and for data acquired during prebolus (a) and main bolus (b). Uncorrected (unc) and corrected (corr) normalized CBV (nCBV) parameter maps were obtained by two different methods (AUC: area under time curve, SVD: singular value decomposition) and their variants (first pass AUC: first pass integration, full AUC: full range integration, standard SVD: standard truncated SVD, Tikhonov SVD: SVD with Tikhonov regularization). The boxes range from the 1st (bottom) to the 3rd (top) quartiles, the red lines indicate the median, notches illustrate the 95% confidence interval of the median, whiskers reach from the minimum to the maximum values within 1.5 times the interquartile range and outliers are displayed as red crosses. The horizontal lines indicate plausible nCBV reference values derived from first pass AUC (Table 1). Please note that for PB data (a) and uncorrected standard SVD processing, nCBV (=46.3%) of one patient (#119) lies outside the plotted range (indicated by a red arrow).

while correction with Tikhonov SVD introduces an insignificant increase in nCBV averages in CET.

Differences between nCBV values obtained from data acquired during prebolus (i.e. without predose) and main bolus (i.e. with predose) are more closely investigated by means of Bland-Altmann plots (Fig. 3). Differences between PB and MB nCBV averages in CET are most impressively reduced by AUC-based methods, where the mean difference is almost zero for first pass AUC. For standard SVD, leakage correction clearly reduces the enormous variance observed for uncorrected nCBV averages in CET, however, the mean values are still significantly different ($-2.78 \pm 3.02\%$) after correction. For Tikhonov SVD, variance and mean differences do not significantly change by introducing correction. Overall, the variance of observed differences between prebolus and main bolus derived nCBV averages (in CET) across patients is much higher in SVD-based methods. The patient means of VOI average nCBV values in CET as well as healthy GM and WM are tabulated in Table 1. Values with insignificant differences between prebolus and main bolus nCBV are highlighted by bold print.

Finally, the Chi-square distance was calculated between nCBV values derived from prebolus and main bolus data to test their accordance for different processing techniques. From box plots of the Chi-square distance (Fig. 4) it is obvious that leakage correction techniques generally increase the accordance between nCBV values obtained from prebolus and main bolus data, but AUC-based techniques clearly outperform the SVD-based techniques with only small differences between first pass and full integration.

Discussion

In this work, we compared normalized CBV values obtained by different processing techniques from data acquired during injection of the prebolus (i.e. without CA predose) and the main bolus (i.e. with CA predose). The investigated techniques were based either on integration of the relaxation time curve (first pass AUC, full AUC) or on singular value decomposition (standard SVD, Tikhonov SVD). In accordance with Hu et al. [8], the nCBV values in leakage-affected tissue, i.e. contrast enhancing tumor) strongly depended on the postprocessing technique and whether or not a predose was applied. Overall, the AUC approach, where leakage correction was performed using linear combinations of reference curves [11,13] revealed consistent nCBV maps (Figs. 1 and S1) and the best accordance between leakage-corrected prebolus and main bolus nCBV values (Table 1). This result was confirmed by the lowest mean differences and variances (Fig. 3b and d) as well as the lowest mean Chi-square distance and its variance (Fig. 4).

Comparing uncorrected and corrected nCBV values, our results demonstrate a consistent up-correction of low uncorrected nCBV values, derived from DSC data acquired from a single dose of contrast agent, i.e. without or in this case during the prebolus (Fig. 2a). This fits well with the known dominance of T1-related leakage effects for single bolus DSC-data especially at rather short TR and large flip angle as in the current study [4,10,26]. For main bolus data (i.e. with predose), uncorrected nCBV values were generally higher than prebolus values and correction effects were generally smaller and inconsistent across methods (Fig. 2b). The down-correction of main bolus, uncorrected AUC-based nCBV values fits with a previously observed predominance of T2*-related leakage effects in data acquired after a predose [13,18,27], where a recent study demonstrated increasing effects with increasing predose [28]. Overall, the reduced influence of correction is in accordance with findings of Paulson and Schmainda [26] who recommended use of a CA preload because it generally minimizes the influence of acquisition and post-processing methods.

Having a closer look at the relative performance of the two investigated methods and their variants, the reference curve-based AUC correction methods [11,13] clearly outperform the SVD based methods [9,13]. This judgment is based on the high consistency between parameter maps (Figs. 1 and S1) as well as corrected nCBV values obtained from PB and MB data for both contrast-enhancing tumor and healthy brain tissue, especially for first pass integration (Table 1, Figs. 2–4). This also fits with results of Spampinato et al. [29] who did not find significant differences between rCBV values obtained by integration of fitted relaxation time curves of two consecutive CA boli. However, they also used a PRESTO sequence with low flip angle, which certainly reduced the influence of T1-related leakage effects. For the SVD-based techniques on the other hand, leakage correction at least reduced the gap between PB and MB nCBV, but did not really achieve a good match (Table 1, Figs. 2–4). This clearly inferior performance can be explained by

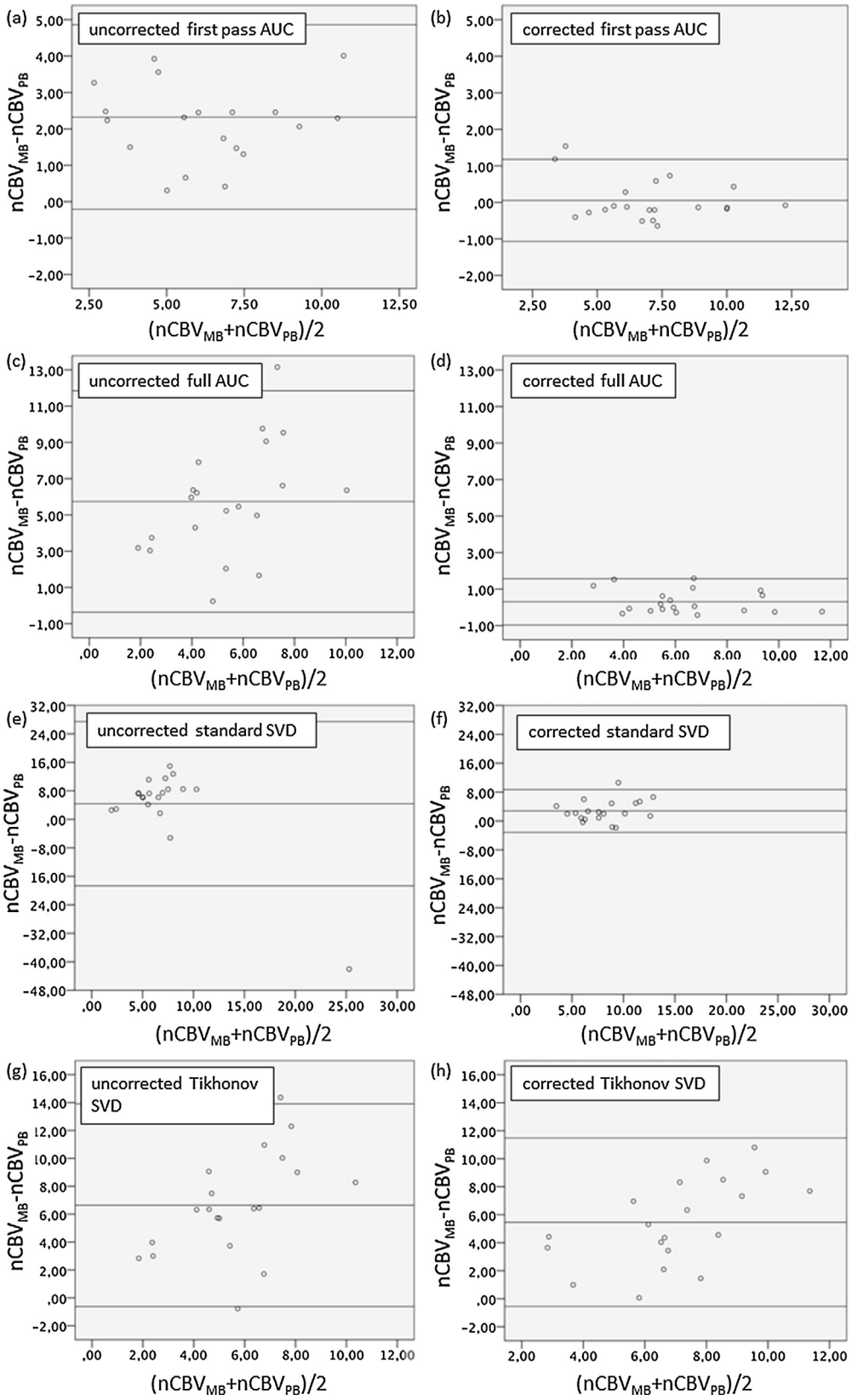

Fig. 3. Bland-Altmann plots comparing normalized CVB values in contrast enhancing tumor of 20 patients obtained from data acquired during the prebolus ($nCBV_{PB}$) and main bolus ($nCBV_{MB}$), respectively. The differences between PB and MB nCBV values ($nCBV_{MB} - nCBV_{MB}$) are plotted vs. their mean values (($nCBV_{MB} + nCBV_{MB}$)/2). The central horizontal line indicates the mean difference between $nCBV_{PB}$ and $nCBV_{MB}$; the lower and upper horizontal lines indicate mean −1.96 SD (standard deviation) and mean + 1.96 SD. Different processing methods are displayed in different panels: (a) uncorrected first pass AUC, (b) corrected first pass AUC, (c) uncorrected full AUC, (d) corrected full AUC, (e) uncorrected standard SVD, (f) corrected standard SVD, (g) uncorrected Tikhonov SVD, (h) corrected Tikhonov SVD. (AUC: area under time curve, first pass: first pass integration, full: full range integration, SVD: singular value decomposition, standard SVD: standard truncated SVD, Tikhonov SVD: SVD with Tikhonov regularization).

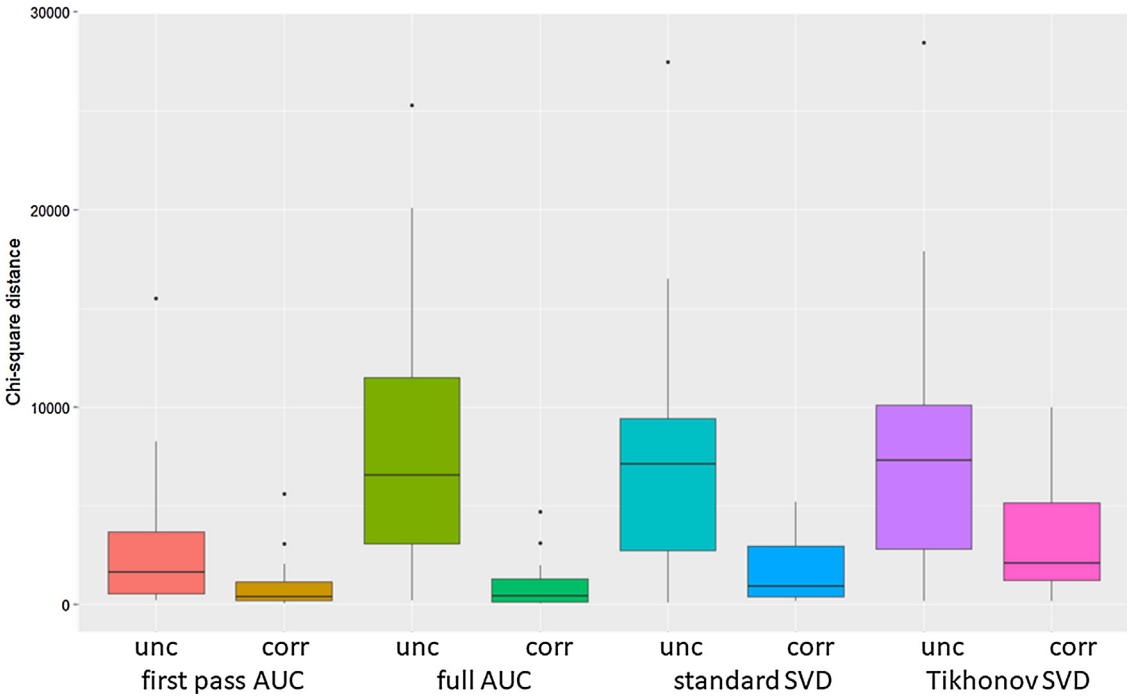

Fig. 4. Box plots of Chi-square distance between nCBV values obtained from DSC data acquired during prebolus and main bolus for different processing methods. Higher values indicate bigger differences between prebolus and main bolus. Uncorrected (unc) and corrected (corr) normalized CBV (nCBV) parameter maps were obtained by two different methods (AUC: area under time curve, SVD: singular value decomposition) and their variants (first pass AUC: first pass integration, full AUC: full range integration, standard SVD: standard truncated SVD, Tikhonov SVD: SVD with Tikhonov regularization).

the well–known noise sensitivity of SVD-based techniques [13,19]. For data acquired during the prebolus, this problem is exacerbated by the low (half) dose of contrast agent (supplement). This also fits with results of Nael et al. [30] who found inferior performance of block-circulant SVD compared to a Bayesian approach at a comparably low CA dose.

Minor influence (compared to CET) of acquisition and leakage correction schemes was observed on nCBV values in unaffected GM and WM (Table 1). As leakage is either estimated as deviation from a previously defined healthy reference curve (AUC) or from averaging the (wiggled) tail of the residue function $R(t)$ (SVD), noise contributions can be expected to affect leakage corrected nCBV values of healthy tissue (without leakage). This effect is stronger for SVD-based methods, which are more susceptible to noise. Likewise, PB-derived nCBV values are more affected because the signal drop is clearly lower (supplemental Fig. S3). However, there are also indications that at least slight leakage might also occur in healthy tissue (see discussion in [13]).

With respect to a generalization of the presented results, there are a few points that need to be kept in mind. Firstly, dissenting from ASFNR recommendations [4], we used a relatively large flip angle of 90° in our GE EPI imaging sequence, which certainly accounted for the rather prominent underestimation of uncorrected nCBV values due to T1-related leakage effects. Secondly, our single-dose nCBV parameter maps were derived from DSC data acquired during application of a half dose prebolus. This resulted in a lower SNR due to a lower signal drop, which is especially obvious for the SVD-based nCBV maps (Fig. 1 and supplement). Thus, a full CA dose would probably be more appropriate for single-dose DSC-MRI. Thirdly, for SVD-based leakage correction, K_2 was calculated by averaging the tail of the impulse response function for $t > 8 \cdot T_c$ (or at least 10 time points) because simulations demonstrated improved accuracy for later thresholds [21]. However, this might increase noise sensitivity compared to the original implementation using $t = T_c$ [9].

Conclusion

The reference curve-based leakage correction approach with integration-based nCBV calculation [11,13] yielded a high accordance between nCBV values obtained without and with prebolus, respectively. It thus appears well suited to obtain valid nCBV values in glioblastoma with a single CA injection.

Ethical approval

All procedures performed in studies involving human participants were in accordance with the ethical standards of the institutional and/national research committee and with the 1964 Helsinki declaration and its later amendments or comparable ethical standards.

Funding

This work was supported by the German Research Foundation DFG [grant numbers PR 1039/4-1, TP: FO 886/1-1]; and the Faculty of Medicine of the Technische Universität München (grant numbers TP: KKF B11-14; BW: KKF).

Author contributions

Conception and design of the study: A.K., C.P.; acquisition of data: D.H., T.P., J.K., B.W.; analysis and interpretation of data: A.K., D.H., B.W., C.Z., C.P.; drafting the article: A.K., C.P., D.H., B.W.; revising the article critically for important intellectual content: T.P., C.Z., J.K.; final approval of the version to be submitted: all authors.

Informed consent

Informed consent was obtained from all individual participants included in the study.

Disclosure of interest

The authors declare that they have no competing interest.

Acknowledgements

The authors thank all patients who participated in this study.

Appendix A. Supplementary data

Supplementary data associated with this article can be found, in the online version, at https://doi.org/10.1016/j.neurad.2018.04.006.

References

[1] Preibisch C, Tóth V, Zimmer C. MR perfusion imaging. In: Hattingen E, Pilatus U, editors. Brain tumor imaging. Heidelberg: Springer; 2016. p. 75–98.
[2] Lee S, Yun TJ, Kang KM, Rhim JH, Park CK, Kim TM, et al. Application of diffusion-weighted imaging and dynamic susceptibility contrast perfusion-weighted imaging for ganglioglioma in adults: comparison study with oligodendroglioma. J Neuroradiol 2016;43(5):331–8.
[3] Theillac M, Meyronet D, Savatovsky J, Makris N, Hannoun S, Grand S, et al. Dynamic susceptibility contrast perfusion imaging in biopsy-proved adult medulloblastoma. J Neuroradiol 2016;43(5):317–24.
[4] Welker K, Boxerman J, Kalnin A, Kaufmann T, Shiroishi M, Wintermark M, et al. ASFNR recommendations for clinical performance of MR dynamic susceptibility contrast perfusion imaging of the brain. AJNR Am J Neuroradiol 2015;36(6):E41–51.
[5] Wiestler B, Kluge A, Lukas M, Gempt J, Ringel F, Schlegel J, et al. Multiparametric MRI-based differentiation of WHO grade II/III glioma and WHO grade IV glioblastoma. Sci Rep 2016;6:35142.
[6] Barajas Jr RF, Chang JS, Segal MR, Parsa AT, McDermott MW, Berger MS, et al. Differentiation of recurrent glioblastoma multiforme from radiation necrosis after external beam radiation therapy with dynamic susceptibility-weighted contrast-enhanced perfusion MR imaging. Radiology 2009;253(2):486–96.
[7] Barajas Jr RF, Cha S. Benefits of dynamic susceptibility-weighted contrast-enhanced perfusion MRI for glioma diagnosis and therapy. CNS Oncol 2014;3(6):407–19.
[8] Hu LS, Kelm Z, Korfiatis P, Dueck AC, Elrod C, Ellingson BM, et al. Impact of software modeling on the accuracy of perfusion MRI in glioma. AJNR Am J Neuroradiol 2015;36(12):2242–9.
[9] Bjornerud A, Sorensen AG, Mouridsen K, Emblem KE. T1- and T2*-dominant extravasation correction in DSC-MRI: part I–theoretical considerations and implications for assessment of tumor hemodynamic properties. J Cereb Blood Flow Metab 2011;31(10):2041–53.
[10] Boxerman JL, Prah DE, Paulson ES, Machan JT, Bedekar D, Schmainda KM. The Role of preload and leakage correction in gadolinium-based cerebral blood volume estimation determined by comparison with MION as a criterion standard. AJNR Am J Neuroradiol 2012;33(6):1081–7.
[11] Boxerman JL, Schmainda KM, Weisskoff RM. Relative cerebral blood volume maps corrected for contrast agent extravasation significantly correlate with glioma tumor grade, whereas uncorrected maps do not. AJNR Am J Neuroradiol 2006;27(4):859–67.
[12] Calamante F, Gadian DG, Connelly A. Quantification of bolus-tracking MRI: improved characterization of the tissue residue function using Tikhonov regularization. Magn Reson Med 2003;50(6):1237–47.
[13] Kluge A, Lukas M, Toth V, Pyka T, Zimmer C, Preibisch C. Analysis of three leakage-correction methods for DSC-based measurement of relative cerebral blood volume with respect to heterogeneity in human gliomas. Magn Reson Imaging 2016;34(4):410–21.
[14] Knutsson L, Stahlberg F, Wirestam R. Aspects on the accuracy of cerebral perfusion parameters obtained by dynamic susceptibility contrast MRI: a simulation study. Magn Reson Imaging 2004;22(6):789–98.
[15] Donahue KM, Krouwer HG, Rand SD, Pathak AP, Marszalkowski CS, Censky SC, et al. Utility of simultaneously acquired gradient-echo and spin-echo cerebral blood volume and morphology maps in brain tumor patients. Magn Reson Med 2000;43(6):845–53.
[16] Knutsson L, Lindgren E, Ahlgren A, van Osch MJ, Bloch KM, Surova Y, et al. Dynamic susceptibility contrast MRI with a prebolus contrast agent administration design for improved absolute quantification of perfusion. Magn Reson Med 2014;72(4):996–1006.
[17] Leu K, Boxerman JL, Ellingson BM. Effects of MRI protocol parameters, preload injection dose, fractionation strategies, and leakage correction algorithms on the fidelity of dynamic-susceptibility contrast MRI estimates of relative cerebral blood volume in gliomas. AJNR Am J Neuroradiol 2017;38(3):478–84.
[18] Hu LS, Baxter LC, Pinnaduwage DS, Paine TL, Karis JP, Feuerstein BG, et al. Optimized preload leakage-correction methods to improve the diagnostic accuracy of dynamic susceptibility-weighted contrast-enhanced perfusion MR imaging in posttreatment gliomas. AJNR Am J Neuroradiol 2010;31(1):40–8.
[19] Ostergaard L, Weisskoff RM, Chesler DA, Gyldensted C, Rosen BR. High resolution measurement of cerebral blood flow using intravascular tracer bolus passages. Part I: Mathematical approach and statistical analysis. Magn Reson Med 1996;36(5):715–25.
[20] Hansen PC. Numerical Algorithms, in Regularization Tools Version 4.0 for MAtlab 7.3; 2007. p. 189–94.
[21] Kluge A. From tissue perfusion to oxygenation: characterizing glioma heterogeneity with dynamic susceptibility contrast enhanced magnetic resonance imaging. München: Fakultät für Medizin: Technische Universität München; 2017.
[22] Leenders KL. PET: blood flow and oxygen consumption in brain tumors. J Neurooncol 1994;22(3):269–73.
[23] Mineura K, Sasajima T, Kowada M, Ogawa T, Hatazawa J, Shishido F, et al. Perfusion and metabolism in predicting the survival of patients with cerebral gliomas. Cancer 1994;73(9):2386–94.
[24] Yushkevich PA, Piven J, Hazlett HC, Smith RG, Ho S, Gee JC, et al. User-guided 3D active contour segmentation of anatomical structures: significantly improved efficiency and reliability. Neuroimage 2006;31(3):1116–28.
[25] Altman DG, Bland JM. Measurement in medicine: the analysis of method comparison studies. J R Stat Soc D 1983;32(3):307–17.
[26] Paulson ES, Schmainda KM. Comparison of dynamic susceptibility-weighted contrast-enhanced MR methods: recommendations for measuring relative cerebral blood volume in brain tumors. Radiology 2008;249(2):601–13.
[27] LaViolette PS, Daun MK, Paulson ES, Schmainda KM. Effect of contrast leakage on the detection of abnormal brain tumor vasculature in high-grade glioma. J Neurooncol 2014;116(3):543–9.
[28] Bell LC, Hu LS, Stokes AM, McGee SC, Baxter LC, Quarles CC. Characterizing the influence of preload dosing on Percent Signal Recovery (PSR) and Cerebral Blood Volume (CBV) measurements in a patient population with high-grade glioma using dynamic susceptibility contrast MRI. Tomography 2017;3(2):89–95.
[29] Spampinato MV, Wooten C, Dorlon M, Besenski N, Rumboldt Z. Comparison of first-pass and second-bolus dynamic susceptibility perfusion MRI in brain tumors. Neuroradiology 2006;48(12):867–74.
[30] Nael K, Mossadeghi B, Boutelier T, Kubal W, Krupinski EA, Dagher J, et al. Bayesian estimation of cerebral perfusion using reduced-contrast-dose dynamic susceptibility contrast perfusion at 3 T. AJNR Am J Neuroradiol 2015;36(4):710–8.